MASTER EM3E-4SW

Academic year 2018-2019

Erasmus Mundus Master in Membrane Engineering for a Sustainable World

Semester 4

Master Thesis Project

Development of Ceramic-Supported 2D Nanosheet Membranes for Organic Solvent Nanofiltration

VILLICAÑA GONZÁLEZ Eduardo

28.06.2019

Supervisor: Marie-Alix Pizzoccaro-Zilamy, m.d.pizzoccaro@utwente.nl; Mieke Luiten-Olieman , m.w.j.luiten@utwente.nl.

Overseer: Reyes Mallada, r.mallada@unizar.es.

www.em3e.eu

"The EM3E4SW Master is an Education Programme supported by the European Commission, the European Membrane Society (EMS), the European Membrane House (EMH), and a large international network of industrial companies, research centres and universities"

"The EM3E4SW education programme has been founded with support from the European Commission. This publication reflects the views only of the author, and the Commission cannot be held responsible for any use which may be made of information contained therein".

Acknowledgments

I would like to express my special thanks of gratitude to my supervisor D.Sc. Marie-Alix Pizzoccaro-Zilamy for her guidance, patience and support during my master thesis assignment. Likewise, I would like to express my gratitude to my co-supervisor Mieke Luiten-Olieman and my overseer Reyes Mallada for their advice and support.

I would like to extend my gratitude to the European Institute of Membranes in Montpellier and the partner universities involved in my formation during this master: University of Montpellier II, University of Chemistry and Technology of Prague, University of Zaragoza, and University of Twente. Also, I would like to thank the European Commission for the economical support.

In addition, I would like to thank the MST cluster at the University of Twente to open to me a space to develop the present work. I also thank to my master colleagues. I express my special gratitude to my friend Sajjad Ghojavand for his friendship, guidance, support, and patience.

Finally, I would like to thank my family for their support from the other side of the ocean. I thank specially to my brother León Fernando and his wife Mirjam Dinkebach, who have been aware of me during these two years from Germany.

Index

Tables Index

Figures Index

1. Introduction

In this first section, the theory and principles behind 2D inorganic nanosheets and their properties are described, followed by methods and tools used to synthetize and manipulated them. Before delving into the aim of this project, the characteristics of nanofiltration (NF) membranes are described and linked to the employment of 2D inorganic nanosheets for the development of new NF membranes. Recent research into 2D inorganic nanosheet based membranes is presented before concluding with the founding concept of this project.

A. 2D-based inorganic nanosheet material

Inorganic nanosheets are plate-like particles with thickness at the molecular dimensions (thickness ≈ 1 nm) and width in the range of several hundreds of nano-meters reaching even the micro-scale [1,2]. Mostly, inorganic 2D-nanosheets are obtained by exfoliation of layered mother crystals [1–4]. The mother layered crystals should possess highly anisotropic 2D crystal structure with strong in-plane bonds and relatively weak out-of-plane bonds to provide an expandable interlayer gallery space. This interlayer gallery is needed by allowing host guest species or solvent molecules to be intercalated between the layers to lead to a proper nanosheet formation [1–3]. These small unit of inorganic crystals can undergo wrinkling, buckling and scrolling thanks to their macroscopic softness resulting from their low thickness (Figure 1). Hence, it is possible to develop a wide range of new materials with different properties by tuning the 2D inorganic nanosheets structure (*electrical, optical, photochemical, and magnetic*) [1].

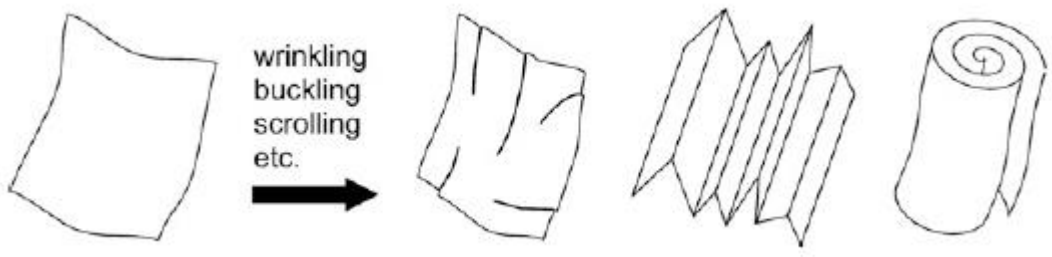

Figure 1. Schematic representation of the possible ways to manipulate the morphology of a nanosheet [1].

Almost all categories of inorganic compounds can form nanosheets [1]. The large surface area and low thickness of inorganic nanosheets enables their hybridization with several guest molecules including organic and inorganic compounds [1,3]. This allows

the tunability of their surface charge, hydrophilicity, smoothness, and interlayer space [1-3].

Research in nanoscience and nanotechnology studied the spontaneous anisotropic growth of 2D inorganic nanosheets [2] by co-precipitation [5,6], hydrothermal synthesis [7,8] and in situ growth [9,10].

Inorganic nanosheets can be classified based on the nature of the mother layered crystals, which are categorized as ion-exchangeable and non-ion exchangeable crystals[1].

Ion-exchangeable layered crystals are composed by electrically charged nanosheets or polyions electrostatically bound through interlayer counterions, which can be exchanged with other ions [1]. Depending on the nature of the interlayer counter-ions, these materials are further classified into cation- and anion- exchangeable layered crystals [1]. Cation-exchangeable crystals include transition element oxometallates, such as niobates, titanates, manganates, metal phosphates, clay minerals, and perovskite-type oxides. Double layered hydroxides (i.e. nickel hydroxide) and hydroxide salts (i.e. $La(OH)_2NO_3$) are included in the anion-exchangeable subgroup [1]. These 2D-nanosheets can build-up composites with potential applications in heterogeneous catalysis, high temperature superconductors, ferromagnetic/ferroelectric films, porous electrode materials, fuel cells, electrochemical sensors, biomolecule/drug reservoirs, photoluminescence material [3], and selective permeation membranes [11].

Non-ion-exchangeable layered crystals can be subdivided into polar and nonpolar or van der Waals (vdW) solids [1]. Nonpolar layered crystals such as transition metal dichalcogenides (e.g., MoS_2, WS_2) are stacked by interlayer vdW forces. These materials cannot be easily exfoliated due the strong interlayer interactions, which hinder the penetration of solvent molecules into the interlayer space. In this case, their variable oxidation state can control the electronic properties rather than combining with other kind of functional groups [1]. Non-ion-exchangeable layered crystals, such as boron nitrides (BN) and MoS_2 nanosheets, can be applied in supercapacitors, oxygen reduction reactions, and lithium-ion batteries [12].

B. Nanofiltration membranes

Before continuing with the recent research into 2D-inorganic nanosheet based membranes, it is important to understand the criteria in which a membrane will be judged as a nanofiltration (NF), an ultrafiltration (UF), or reverse osmosis (RO) type membrane. For this reason, standard definition relevant to this project are briefly highlighted below.

NF membranes possess properties between UF and RO [13,14]. According to IUPAC recommendations, both UF and NF are pressure driven membrane based separation processes, where the pore size and rejections properties make the difference [15]. UF membranes are able to reject particles and dissolved macromolecules between 2 – 100 nm [15]. NF membranes have pore sizes smaller than 2 nm, being thus ideal for the removal or recovery of organic molecules from water or solvents [11]. NF membranes are applied frequently to remove pathological microorganisms, biological sludges from treated water, and biological compounds (i.e. undesired metabolites and toxins)[14,16]. RO is a liquid phase pressure driven separation process, where the transmembrane pressure causes the selective diffusion of solvents through a membrane, against the osmotic pressure difference. As RO membranes, NF membranes are efficient for the removal of inorganic salts [15]. In comparison, NF membranes present lower rejection of monovalent ions, higher rejection of divalent ions, and higher flux [14]. This selective separation properties are possible because NF membranes present also functional groups on the surface. Therefore, the sieving mechanism is complemented by a combination of electrostatic and steric interactions associated with charge shielding, Donnan exclusion, and degree of ion hydration [13,14].

There are important intrinsic factors in a nanofiltration membrane, which affect their desired performance. An ideal membrane would present a finely tailored pore size, high porosity, and a thickness as low as possible in order to maximize the flux with a rejection of solutes near 90 %. Two-dimensional inorganic nanosheet membranes (2D-NSMs) have opened up a new approach to get size-selective molecular separation membranes with ultrafast permeation, good mechanical strength and good rejection properties [11,17].

It is noteworthy that the lower carbon footprint and smaller spatial requirements of 2D-NSMs, in comparison with conventional NF membranes, makes them promising systems for application in industry (such like petrochemical, food, pharmaceutical, and water treatment industries) [11]. Moreover, it is well known that membrane separation

processes have lower energy requirements due the lack of a phases transition and additives as in distillation [11].

C. 2D inorganic nanosheet based membranes

2D inorganic nanosheets have been employed as nano-building blocks for development of separation membranes with unique intergallery nanochannels [18]. In such membranes, the mass transport takes place at the interlayer space rather than the intralayer space alike in conventional ultrafiltration and nanofiltration (UF/NF) membranes [19]. As schematically represented in Figure 2, the solvent transport (*small blue circle*) is possible thanks to the multichannel inner structure of the membranes formed from the disordered self-assembling of the nanosheets (*represented in green*) on a porous support (*in grey*) [5,19]. The rejection of the solutes (*large blue circle*) is a result of the narrow intergallery diffusion channels [5]

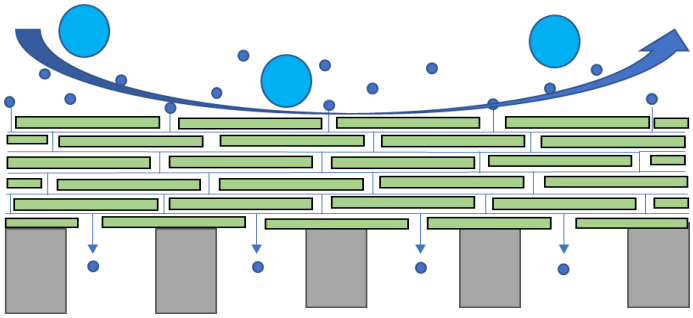

Figure 2. Schematic representation of 2D-NSMs structure and transport/separation mechanism: in grey the porous support; in green the deposed 2D inorganic nanosheets; in dark blue the solvent; in light blue the solute.

In general, 2D nanosheet based membranes have shown ultrafast permeance in comparison with conventional/commercial UF/NF membranes; also, they present high selectivity towards organic molecules, such as antibiotics, amino acids, and proteins in the range 0.5-5 nm wide and molecular weights ranging from 500 $g.mol^{-1}$ to 10 000 $g.mol^{-1}$ [11]. Recent research work has shown that 2D inorganic nanosheet membranes achieved ultrahigh flux with permeances over 1000 $L\ h^{-1}\ m^{-2}\ bar^{-1}$, dyes rejection over 90 %, and molecular weight cut-off (MWCO) values of 328 $g.mol^{-1}$ [6,19].

Moreover, by tuning the size of the nanosheets, the interlayer distance between the nanosheets, the composition, and the thickness of the selective layer it is possible to adjust the performance of 2D-NSMs [19].

2D-NSMs have shown promising performance. However, high rejection and flux has been only attained with measurements conducted in dead-end configuration [11].

C.1. Transport theory behind 2D-NSMs

Conventional/commercial NF/UF membranes are composed of thick layers of selective polymeric materials with low porosities and broad pore size distribution. According to the Hagen-Poiseuille equation, the solution flux is proportional to the pressure difference (ΔP) across the membrane and the porosity (ε), and it is inversely proportional to the membrane thickness (L) (Equation 1). Consequently, to obtain high flux through a membrane, the thickness and porosity of the selective layer are critical parameters to control [11].

$$J = \frac{\varepsilon \Delta P d^2}{32 \mu L} = \frac{\varepsilon \Delta P \pi r^2}{8 \mu L} \quad \textbf{(1)}$$

Where μ is the viscosity of the solvent, d is the pore diameter, and r is the pore radius.

Basically, 2D-NSMs design is based on the basic membrane separation theory, where the separation process is driven by chemical potential gradients such as pressure, temperature and concentration gradients. 2D-NSMs could be analysed by two different models. In one hand, the solution-diffusion model describes the mass transport phenomena through dense membranes without pores or with extremely small pores sizes bellow 0.5nm and the transport mechanism is based on diffusion mechanism of the targeted molecule under a driving force [11].

The pore flow model considers that the membrane flux is affected by the porosity, operating pressure, pore diameter, and thickness of the selective layer. This model is applied in processes involving membranes with tiny pores from the nanoscale to the microscale, which appears to fit better with the separation mechanism of 2D-NSMs. Nevertheless, due the lack of appropriate and accurate characterization techniques, it is hard to obtain the real thickness and porosity of 2D-NSMs, hampering the quantitative analysis of mass transfer across the membrane [11].

C.2. Preparation of 2D-NSMs

2D-NSMs have been fabricated from a wide variety of 2D-layered materials, such as graphene-based materials, transition metal dichalcogenides, covalent organic

frameworks, metal-organic frameworks (MOFs), MXenes, LDH, and layered silicates [20].

Because of the presence of charged functional groups on the surface of 2D-materials like oxygen and nitrogen, the nanosheets can be well dispersed in water. By this way, it is possible to prepare a membrane by three different assisted self-assembly methods: vacuum assisted filtration (VAF), pressure assisted filtration (PAF) or evaporation assisted self-assembly (EASA) (Figure 3). As a result, the nanosheets are deposited together almost parallel to the membrane. The thickness of the membrane can be adjusted by changing the volume or the concentration of the nanosheet dispersion[20]. Tsou and co-workers [21] tested the three assisted self-assembly methods and obtained the best performance with the PAF thanks to the high ordered laminated final structure of these membranes.

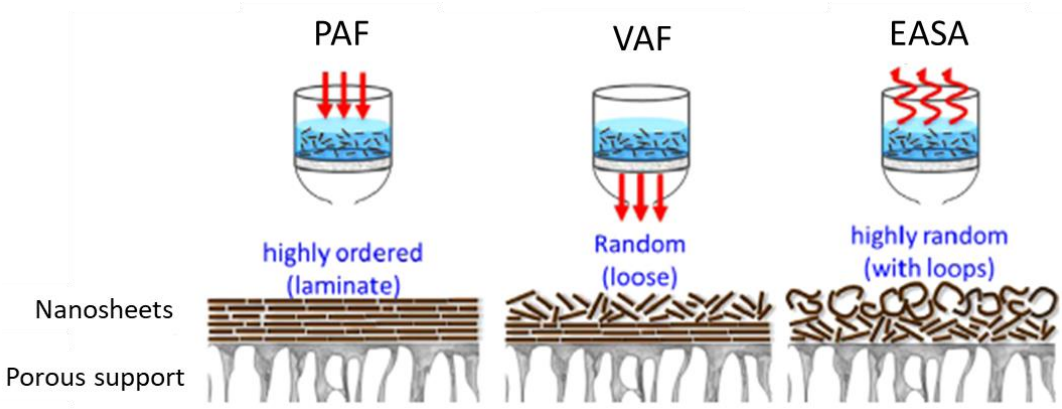

Figure 3. Schematic diagram of the deposited layered structures on a porous support through the three different assisted self-assembly methods described. (Adapted from [21]).

C.3. Characterization of 2D-NSMs

In order to characterize the structure and the separation process mechanism, the 2D-NSMs can be analysed with static and dynamic techniques. Static characterization methods will give us information related to the morphology of the separation layer, composition and thickness, while dynamic methods help us to analyse the permeation, rejection, and pore size of the membrane to characterize its performance [22].

Within the static techniques, one of the most useful characterization tools is scanning electron microscopy (SEM). With this technique several information about the morphology of the membrane can be obtained such as the top surface, the cross-section

and the support/membrane interphase [5,6,9,10,23–25]. Higher resolution technique can be used to confirm the information obtained by SEM, such like, field emission scanning electron microscopy (FESEM), atomic force microscopy (AFM), and scanning transmission electron microscopy (STEM) [6,22].

To get information about the composition and crystallinity of 2D-NSMs, Fourrier Transform infrared (FTIR) spectrometry and X-ray diffraction (XRD) can be employed [5,6,9,10,23–25].

The membrane performance can be characterized by solvent permeation measurement. Dyes rejection and polyethylene glycol molecular weight cut-off (PEG-MWCO) can give information about the selectivity of the membrane. Moreover, since we know the size of the molecules which pass through and which are retained, it is possible to estimate the mean the pore size of the separation layer. Also, with these techniques it is possible to get an idea about the mass-transfer mechanism through the 2D-NSMs. More information be obtained via these techniques, such like, influence of the thickness in the performance, stability of the membrane in function of the time, optimal operation parameters (pressure, temperature), and so on [5,6,9,23,24].

D. Project concept

Several research works have been developed for the preparation of ultra-high flux 2D inorganic nanosheet based membranes. Figure 4 shows a performance comparison of selected 2D inorganic nanosheets membranes with graphene, graphene oxide (GO) and polyether sulfone membranes (PES). From this figure it is possible to see that nickel hydroxide ($Ni(OH)_2$) and boron nitride (BN) 2D nanosheet membranes present the highest permeability ($\approx$ 1100-1300 L $h^{-1}m^{-2}bar^{-1}$) without compromising the high selectivity on conventional nanofiltration membranes ($\geq$ 90%).

Therefore, the aim of this project is to reproduce the work reported in literature with $Ni(OH)_2$ and BN based membranes to confirm the performances reported and understand better the properties and the transport/separation mechanism of these membranes. In addition, this will allow us to develop reproducible and clear protocols for the preparation of such membranes. Before to get more in details in the preparation methods and results obtained, a quick overview of these materials selected are provided in this section.

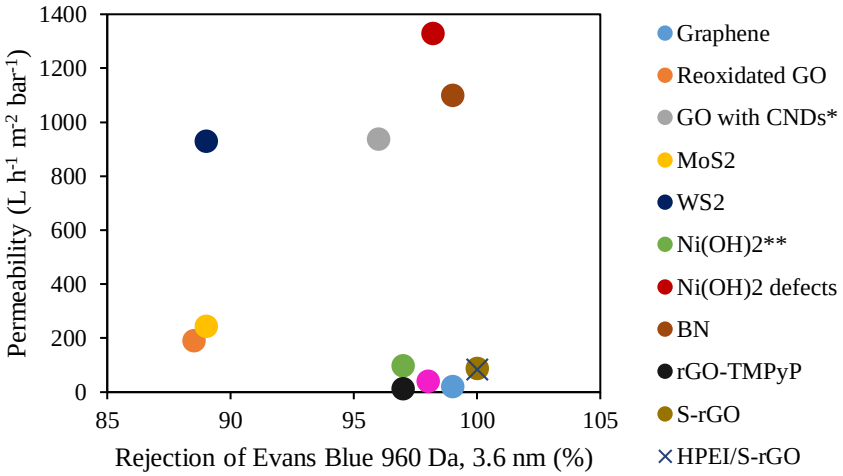

Figure 4. Comparison of the performance of different 2D inorganic nanosheets membranes with graphene, graphene oxide and polyether sulfone. *Rejection for rhodamine B (RB), 479 Da, 1.6 nm. **Rejection for direct yellow (DY), 957 Da, ***Victoria Blue (VB), 458 Da.

D.1. Membranes based on $Ni(OH)_2$ nanosheets.

Nickel hydroxide is an organic layered material, categorized within layered double hydroxides (LDHs) (Figure 5). These materials are typical representatives of crystalline layered compounds and have the general formula described in Equation 2.

$$[M^{2+}_{1-x}M^{3+}_{x}(OH)_2][A^{n-}]_{x/n} \cdot zH_2O \quad \textbf{(2)}$$

Where, M^{2+}, M^{3+} represent di- and tri-valent metal ions respectively, A^{n-} *n*-valent ions, and H_2O the interlayer water [25]. In these materials, metal cations are located at the centre of edge sharing octahedra, whose vertices contain hydroxide ions that connect to form infinite brucite-like 2D layers. Unlike stacked graphene or GO sheets, the interlayer spacing of LDHs is highly uniform and can be adjusted by a proper intercalation of compensation anions [25].

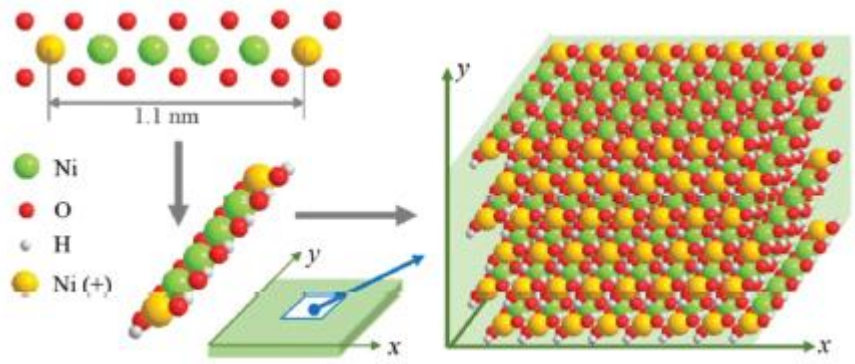

Figure 5. Schematic representation of the 2D-layered structure of $Ni(OH)_2$ proposed by Qu et al [5].

Qu and co-workers [5] reported the first $Ni(OH)_2$ nanosheet based membrane (NiNM). The nanosheets were synthetized by coprecipitation and final dispersion was employed to make the membrane by vacuum assisted filtration. Such membranes were reported to have a permeability of 99 L m^{-2} h^{-1} bar^{-1} with good rejection for several dyes in aqueous solution: of 77.4% for 1,10-Phenantrinin monohydrate (Phen), 94.7% for methylene blue (MB), 86.4% for methyl orange (MO), 97.3% for direct yellow (DY), and 100% for TMPyP[1]. From these values, they determined a MWCO of 328 g mol^{-1}. Moreover, the membrane presented good permeability for organic solvents, such as hexane (841 L m^{-2} h^{-1} bar^{-1}), toluene (300 L m^{-2} h^{-1} bar^{-1}), and ethanol (175 L m^{-2} h^{-1} bar^{-1}). It was found that the viscosity of the solvent is an important parameter influencing the permeability of the membrane.

Ang and co-workers [6] on the other hand, prepared a NiNM with controlled structural defects in the nanosheets structure in order to enhance the permeability of the membrane while keeping the same selectivity properties. The 641 µm thick defect-rich membrane achieved a water permeance of 1330 L m^{-2} h^{-1} bar^{-1}, while the dyes rejection was kept over 90% for methyl red (MR), MO, rhodamine B (RB), and Evans blue (EB).

D.2. Membranes based on functionalized boron nitride nanosheets (FBNNs)

Hexagonal boron nitride (*h*-BN) is analogue of graphite with some unique properties, such as higher specific surface area, higher structural defects, chemical inertness, and high resistance to oxidation. This chemical inertness makes of *h*-BN a hard material to intercalate or exfoliate [26]. Commercial *h*-BN has been functionalized with amine functional groups ($-NH_2$) by exfoliation of the nanosheets in presence of urea leading to functionalized boron nitride nanosheets (FBNNs) (Figure 6) [19,27]. Such type of material has been employed to prepare supported 2D nanosheets membranes applied in OSNF [19], water cleaning [28], and nanofluidic electric generators [29].

The FBNNs membrane presented an ultrahigh solvent permeability for acetone (1660 L h^{-1} m^{-2} bar^{-1}), water (620 L h^{-1} m^{-2} bar^{-1}), methanol (≈1375 L h^{-1} m^{-2} bar^{-1}), and dimethylformamide (≈1250 L h^{-1} m^{-2} bar^{-1}). The 1 µm thick membrane showed rejection

[1] α,β,γ,δ-tetrakis (1 methylpyridinium-4-yl)porphyrin p-toluenesulfonate

rate of 94.1% for MB, up to 99% for RhB, and 98.5% for R6G (all dyes were dissolved in water) [19].

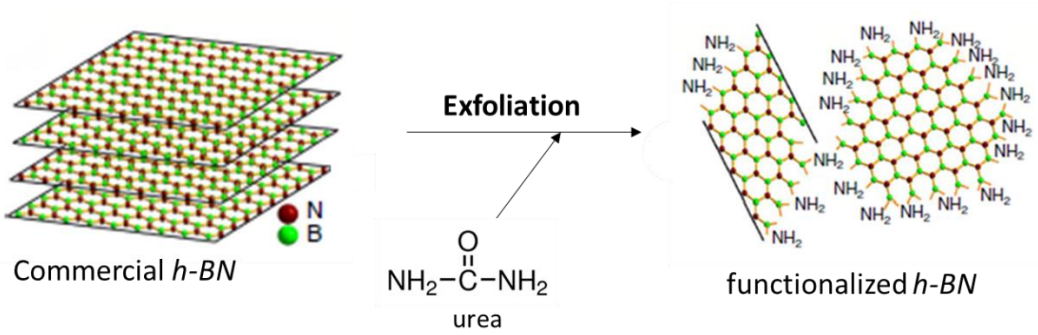

Figure 6. Schematic representation of the exfoliation of *h*-BN in presence of urea to get functionalized BN nanosheets (Adapted from [27]).

2. Experimental

A. Materials

Nickel nitrate hexahydrate ($Ni(NO_3)_2 \bullet 6H_2O$), methylene blue (MB), Hexamethylenetetramine (HMT), sodium dodecyl sulphate (SDS), N,N-dimethylformamide (DMF), hexagonal boron nitride (*h*-BN), ethanol (anhydrous and technique), and urea were purchased at Merck. Polyethylene glycol (PEG) with different molecular weights (300, 600, 1000, 1500, and 3400 $g.mol^{-1}$) were purchased at Merck and used for the Molecular Weight Cut-Off (MWCO) measurements. All chemicals were used as received without any further purification. Ultrapure Millipore water was employed for the synthesis. Polyether sulfone (PES) filter ($Ø_{pore} \approx$ 200 nm, 4.7 cm in diameter) was purchased from PALL. Commercially available, polished α-Al_2O_3 discs (diameter 39 mm, thickness 2 mm, porosity 35%, and $Ø_{pore} \approx$ 80 nm) were supplied from Pervatech B.V the Netherlands.

B. Preparation of the 2D Nanosheet Dispersion

B.1. 2D Nickel hydroxide ($Ni(OH)_2$) nanosheet dispersion.

The procedure to prepare the 2D nickel hydroxide nanosheet dispersion is based on the work of Wang and co-workers[7].

First, layered-like nickel hydroxide crystals were prepared by mixing 1.4 mL of an aqueous $Ni(NO_3)_2.6H_2O$ solution (68.8 mmol L^{-1}, 0.1 mmol), 5.7 mL of an aqueous SDS solution (69.3 mmol L^{-1}, 0.4 mmol), 4.2 mL of an aqueous HMT solution (71 mmol L^{-1}, 0.3 mmol), and 8.7 mL of deionized water. Then, the mixture was stirred 10 min at room

temperature and added to an autoclave which was filled with N_2, closed with PFTE cap, sealed and heated at 120°C for 12 h. The crystal suspension was filtered and then washed twice with 20 mL of deionized water, and one time with 20 mL of anhydrous ethanol. The green powder obtained was then dried at room temperature (m = 11.2 mg, η = 16 %).

In the second step of the synthesis, the exfoliation of the layered-like Nickel hydroxide crystals was conducted by mixing 35 mg of the powder with 35 mL of DMF under stirring and N_2 atmosphere at 60°C during 48h. The resulting dispersion was then centrifuged to remove the remaining non-exfoliated $Ni(OH)_2$ at 6000 rpm for 20 min. From the sediment, the final concentration of the suspension with exfoliated $Ni(OH)_2$ was estimated (0.34 mg/mL). A schematic description of the synthesis process can be found in Figure A. 4.

B.2. Functionalized boron nitride

The functionalized *h*-boron nitride (BN) nanosheets dispersions were prepared based on the procedure described by Chen and coworkers [19]. 0.5 g (0.02 mol) of commercial *h*-BN powder was functionalized and exfoliated using 10 g (0.17 mol) of urea under one dimensional milling with zirconia milling ball (12 mm in diameter) at 200 rpm during 62h at room temperature. Then, the mixture of powders was separated from the milling ball and washed with 400 mL of milli Q water. The aqueous dispersion was dialyzed (in dialysis tubing, MWCO ≈ 10 kDa, $Ø_{internal}$ = 35mm) for 1 week to remove the excess of urea. Finally, the functionalized BN dispersion was centrifuged for 10 min at 3000 rpm to remove the non-exfoliated *h*-BN. The final dispersion concentration was around 0.086 mg mL^{-1}. A schematic description of the process can be found in Figure A. 6.

C. 2D Membrane Preparations

C.1. Assisted Vacuum filtration

For both materials, FBNNs and $Ni(OH)_2$, the dispersions containing the nanosheets or the layered crystal are deposed on the porous support surface by assisted vacuum filtration. The building blocks self-assemble on the surface of the support (PES or α-Al_2O_3). The volume of the dispersion filtrated controls the thickness of the formed separation layer. Table 1 describes the different membranes prepared by vacuum assisted filtration, the support employed, and the volume of dispersion employed for each case according to the kind of material and it is estimated concentration.

Table 1. Summary and description of the membranes prepared by assisted vacuum filtration.

Membrane	Support Material	Volume employed (mL)	Concentration of nanosheets in dispersion (mg mL^{-1})	Sample abbreviation
Layered $Ni(OH)_2$	PES ($Ø_{pore} \approx 200$ nm)	10	0.06	NiLM-1
		10	0.11	NiLM-2
		10	0.17	NiLM-3
		10	0.56	NiLM-4
	α-Al_2O_3 ($Ø_{pore} \approx 80$ nm)	5	0.56	NiLM-α
Exfoliated $Ni(OH)_2$	α-Al_2O_3 ($Ø_{pore} \approx 80$ nm)	5	0.34	NiEx
FBNNs	PES ($Ø_{pore} \approx 200$ nm)	60	0.06	FBNMs

C.3. In situ growth.

To make the in-situ growth on a ceramic support, first we mixed 4.2 mL of an aqueous $Ni(NO_3)_2$ solution (68.8 mmol L^{-1}, 0.3 mmol), 12.6 mL of an aqueous HMT solution (71 mmol L^{-1}, 0.9 mmol), and 43.2 mL of deionized water. After mixing at room temperature for 10 min, the solution was transferred with an α-Al_2O_3 support to an autoclave, which was filled with N_2, closed with PFTE cap, sealed and heated at 120°C for 12 h. A schematic representation of this process can be found in Figure A. 5. Once the reaction finished, the final membrane was rinsed with 20 mL of Milli Q water three times and once with 20 mL of anhydrous ethanol. Finally, the membrane was air dried at room temperature.

D. Characterizations

SEM images were obtained with a JEOL-6010LA low resolution scanning electron microscope using an accelerating voltage of 5 kV. Polymeric membrane samples were prepared by immersion in liquid nitrogen in order to prepare clean cross-section. All the SEM samples were metalized by sputtering a layer of 5 nm Pd/Pt to favour charge release. FTIR analysis was conducted on a Perkin Elmer Spectrum 100 spectrometer. Spectra were recorded in the 4000-600 cm^{-1} range using 16 scans at a nominal resolution of 4 cm^{-1} in ATR mode (pristine porous supports were used as background). X-ray diffraction analysis were performed with a Bruker D2 diffractometer at the wavelength of Cu Kα1 (λ = 1.5405 Å) (30 kV and 10 mA) in Goniometer scanning mode. The program scanned angles (2θ) from 5 to 50 with a 0.020° step, and a step time of 80 s. STEM-in-SEM images

were obtained with a Zeiss Merlin HR-SEM using an accelerating voltage of 30 kV. The samples were prepared by deposing 2 µL of the nanosheet dispersions on a copper grid. Dynamic light scattering (DLS) technique was carried out with a Malvern Zetasizer Nano ZS instrument to estimate particle size distribution. Although DLS analysis is not exact, since the equipment measures the particle size assuming a spherical shape of the particle, it gives a good approximation.

E. Membrane performance

Membranes were tested in a dead-end set-up for liquids, consisting of a stainless-steel feed vessel. During the water permeation/filtration tests, the temperature was kept at 25°C. The feed vessel was connected to the inlet of the membrane module, which led to the active membrane area. The permeate was collected in a test tube and measured at specific intervals (depending on the support) while applying a nitrogen pressure of 0.5, 1, and 1.5 bar in the case of the membranes supported on PES; and 4, 5, 6, and 7 bar for the membranes supported on α-Al_2O_3. The permeate was kept atmospheric. The water permeability [L m^{-2} h^{-1} bar^{-1}] was then calculated as the slope of the flux [L m^{-2} h^{-1}] as a function of the trans membrane pressure [bar]. Each measurement was repeated 3 times for each sample.

Retention analysis with aqueous polyethylene glycol solutions (PEG, Merck) was done using PEGs with different molecular weight (300, 600, 1000, 1500, and 3400 g mol^{-1}) in a dead-end filtration set-up at a transmembrane pressure of 0.5 bar for the polymeric supported membranes and 5 bar for the ceramic supported membranes. A feed volume of 1 L was used with a concentration of 3 g/L (0.6 g/L for each PEG). During the experiment, the liquid was continuously stirred at 300 rpm in order to avoid the occurrence of concentration gradients. During each test, samples of the feed, retentate and permeate solutions were collected once the flux reached a steadying state (approximatively after 1 h, at around 10% of recovery). Analysis of the composition of these samples was conducted by gel permeation chromatography (GPC, Water).

Rejection of dyes was carried out in a dead-end filtration set-up at a transmembrane pressure of 0.5 bar for the polymeric supported membranes and 5 bar for the ceramic supported membranes. As feed, 1 L of methylene blue (MB) aqueous solution with a concentration of 20 ppm (20 mg/L) was employed. During each test, samples of the permeate were collected by intervals of 1 mL, also a sample from the feed and retentate

were taken. A UV-Vis spectrophotometer measured the light absorbance of the samples to get the concentration.

Equation 3 determines the rejection in both measurements, methylene blue retention and PEG-MWCO.

$$R = \left(1 - \frac{C_P}{C_R}\right) * 100 \quad \textbf{(3)}$$

Where R is the rejection of the compound of the dye, and C_R and C_P are the concentrations of the dye in the retentate and the permeate respectively.

3. Results and discussion

A. 2D-based $Ni(OH)_2$ membranes

A.1. 2D $Ni(OH)_2$ nanosheets dispersion

First the procedure described by Qu and workers was used to prepare Nickel Hydroxide nanosheet dispersion [5] by the quick addition of a basic aqueous solution to a nickel (II) nitrate aqueous solution. Unfortunately, independently of the synthesis parameter tested, it was impossible to control the reproducibility of the nanosheets and membranes preparation (Figure A. 3). These irreproducible results are due to the impossibility to control the spontaneous nucleation during co-precipitation at room temperature [30]

In order to achieve more control of the width and crystallinity of the 2D $Ni(OH)_2$ nanosheets, thermal treatment in hydrothermal conditions was conducted on the dispersion during $Ni(OH)_2$ precipitation. This procedure requires the use of hexamethylenetetramine (HMT) as the alkaline reagent, which at high temperatures decomposes into formaldehyde and ammonia and yields to large layered crystallites [31,32]. Besides, the reaction is carried out in presence of sodium dodecylsulfate (SDS) surfactant. The anionic part (dodecylsulfate (DS)) complexes with the Nickel atoms (Ni^{2+}) of the layered $Ni(OH)_2$ structure [8]. Intercalation of surfactant has been used in previous works to control the interlayer spacing [7,8]. After the hydrothermal treatment, the resulting layered $Ni(OH)_2$ crystal was exfoliated to obtain a dispersion of individual nanosheets.

The product obtained was analysed by X-ray diffraction (XRD). Figure 7 A shows the XRD pattern. The peaks obtained at 7, 10, and 14° are in accordance with the results reported in the literature for layered $Ni(OH)_2$ structure [7,8]. Because the XRD configuration was not set for low angle XRD analysis ($2\theta < 5°$), the determination of the interlayer space was not conducted (*peak at 2θ 4° corresponding to the diffraction plan (001)*) [7]. The 2D $Ni(OH_2)$ nanosheets obtained after exfoliation were not analysed by X-ray diffraction due the low quantity of powder obtained (<20 mg).

The composition of the layered $Ni(OH)_2$ crystal was further confirmed by FTIR analysis. The FTIR spectrum shown in Figure 7 B presents the bands related to the dodecyl sulphate surfactant in the layered structure at 2923 and 2984 cm^{-1} which can be assigned to the bending vibrations of $-CH_3$ and $-CH_2$ group respectively. The band at 1193 cm^{-1} is attributed to the stretching vibration mode of sulphate functional group ($-OSO_3^-$) [8].

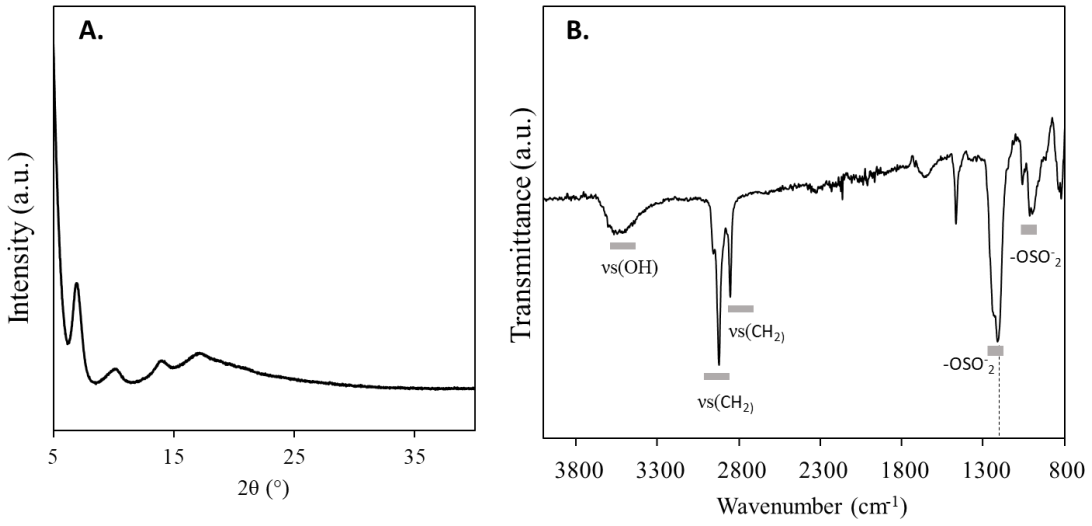

Figure 7. Layered $Ni(OH)_2$ crystal composition and morphology characterization. (A.) XRD pattern. (B.) FTIR spectrum.

STEM-in-SEM analysis was used to characterize the morphology and the size of the 2D nanosheets. Figure 8 shows the STEM-in-SEM image. The nanosheets present an irregular shape, similar to the morphology obtained by Wang and co-workers [7]. However, some nanosheets tend to form an hexagonal crystalline shape, as reported by Ida *et al.* [8] (notation no. 3 and 4 in Figure 8). The differences in morphology are a result of the hydrothermal treatment and exfoliation time differences [7,8].

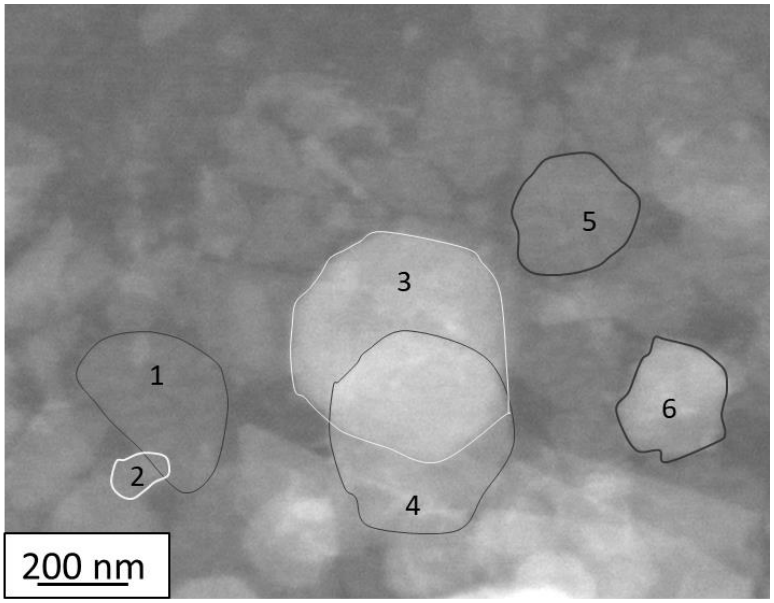

Figure 8. STEM-in-SEM image of $Ni(OH)_2$ nanosheets.

To determine the particle size distribution, DLS analysis was conducted and the results were compared with the distribution obtained using the STEM-in-SEM image (Figure A. 7). Figure 9 A shows the DLS results in terms of number vs size. The DLS size distribution obtained starts at 102 nm and finishes at 712 nm, with a maximum particle concentration at 255 nm. However, DLS analysis gives just an estimation of the size from the light scattered during the measurement based on the presence of only spherical particles. Hence, the analysis by electronic microscopy can corroborate better the particle size and shape. Figure 9 B shows the particle size distribution obtained from the STEM-in-SEM image and using the ImageJ software. The size distribution obtained starts at 100 nm and finishes at 1200 nm, with a maximum concentration of particles width between 100-200 nm. It must be noted that ImageJ provide only a qualitative indication due the lack of differentiation between overlaid nanosheets (i.e. nanosheets no. 1 to 4 in Figure 8). Wang and co-workers [7] reported to had obtained single nanosheets from ≈10 to ≥100 nm in width and thickness of 1 ±0.2 nm by atomic force microscopy (AFM). Also using AFM, Ida and co-workers [8], by following a similar process, reported to have an average size of 585 nm in width, and a thickness of 1.1 nm. The width of the resulting nanosheets is thus large enough to form a membrane on a microporous support.

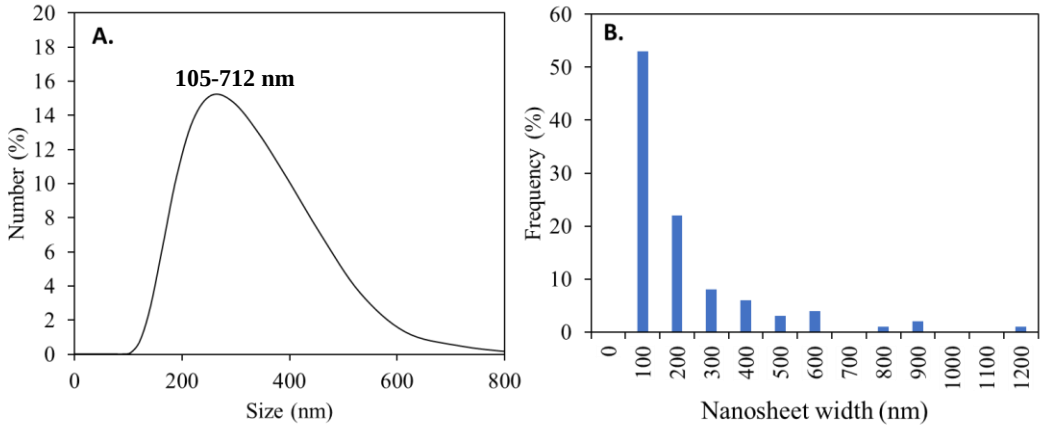

Figure 9. Particle size distribution of $Ni(OH)_2$ nanosheets dispersion. (A.) DLS analysis. (B.) STEM image analysis.

The synthesis of 2D $Ni(OH)_2$ nanosheets by exfoliation of a crystal prepared in hydrothermal condition in presence of a surfactant is a better approach to obtain reproducible nanosheets in terms of size width. Furthermore, it allows a better control of the final nanosheets structure.

A.2. 2D $Ni(OH)_2$ membranes prepared by vacuum assisted filtration

A.2.1 Layered $Ni(OH)_2$ crystal membranes (NiLMs)

To demonstrate the interest to use a 2D $Ni(OH)_2$ nanosheet dispersion instead of a layered $Ni(OH)_2$ crystal dispersion, 4 type of membranes were prepared by vacuum assisted filtration on top of PES support ($Ø_{pore} \approx 200$ nm) and were denoted NiLM. Different concentration (Table 1) were tested to study the influence on the membrane thickness and water permeability. SEM observations were used to study the morphology, location, and homogeneity of the NiLMs. The membrane obtained with the highest concentration of layered $Ni(OH)_2$ (0.45 mg cm^{-2}) presented a thickness of 2 µm and an homogeneous surface as shown in Figure 10. The cracks presented in the top surface are a result of the SEM sample preparation. The cross-section in Figure 10 B show the formation of a laminated membrane formed by layered crystals entangled with each other.

The water permeability results are presented in Figure 11. As the concentration of layered $Ni(OH)_2$ crystal material increases on the forming layer, the flux decreases. For the highest concentrated membrane, non-flux could be measured, suggesting the presence of a thicker layer, thus an increase of the membrane tortuosity.

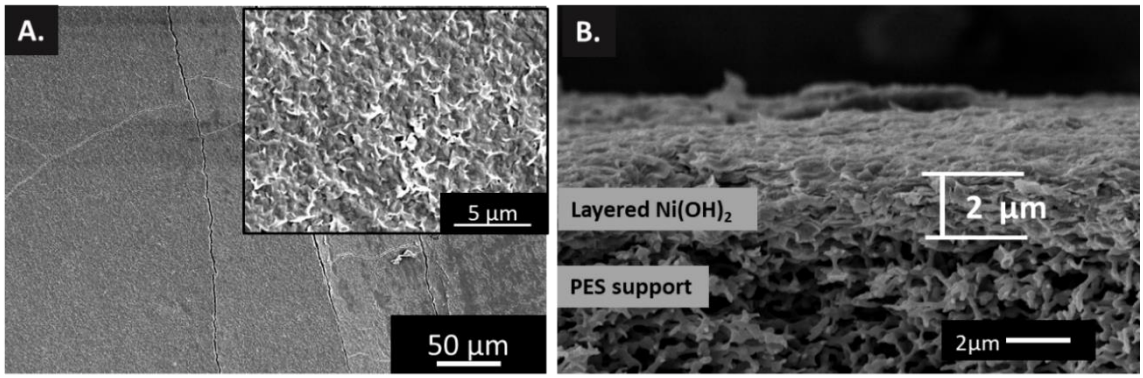

Figure 10. SEM images from layered $Ni(OH)_2$ on PES support. (A.) Top surface of membrane with highest layered crystal concentration. (B.) Cross section of membrane with highest layered crystal concentration.

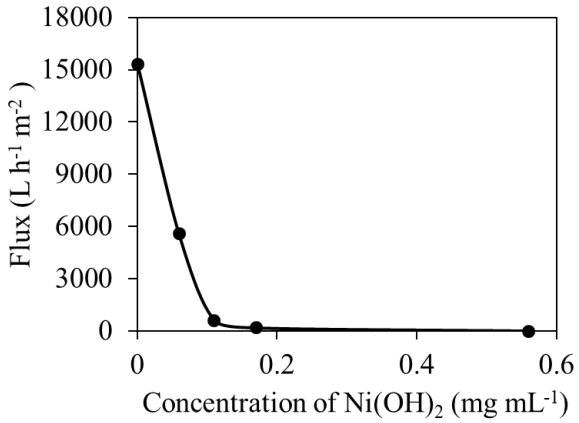

Membrane	Concentration (mg mL^{-1})	Thickness (µm)	Permeability (L h^{-1} m^{-2})
PES-Support	0	0	15319
NiLM-1	0.06	0	5572
NiLM-2	0.11	0.62	609
NiLM-3	0.17	1.20	179
NiLM-4	0.56	2.00	0

Figure 11. Water permeation of layered $Ni(OH)_2$ crystal membranes for different concentrations of deposed material on PES support at 0.5 bar.

Finally PEG retention measurements were conducted on the NiLM in the NF range (solution of PEG with Mw from 200 to 1000 Da). No rejection were observed in the NF range confirming thus the interest of the utilization of 2D $Ni(OH)_2$ nanosheet dispersion (Figure A. 10).

A.2.2. 2D $Ni(OH)_2$ nanosheet membranes

To prepare the 2D $Ni(OH)_2$ nanosheet membranes (NiEx) by vacuum assisted filtration, porous α-Al_2O_3 supports ($Ø_{pore}$≈80 nm) were employed due to the incompatibility of the PES support with the solvent used for the exfoliation. SEM images where used to characterize the morphology of the NiEx membrane. Figure 12 A. shows the homogeneous surface of the membrane. The layered surface present less roughness than the NiLM. Also, Figure 12 B shows the cross section of the membrane with a thickness around 0.7 µm. In this case, it is not possible to distinguish the laminated structure as in the membrane done with layered $Ni(OH)_2$ crystals.

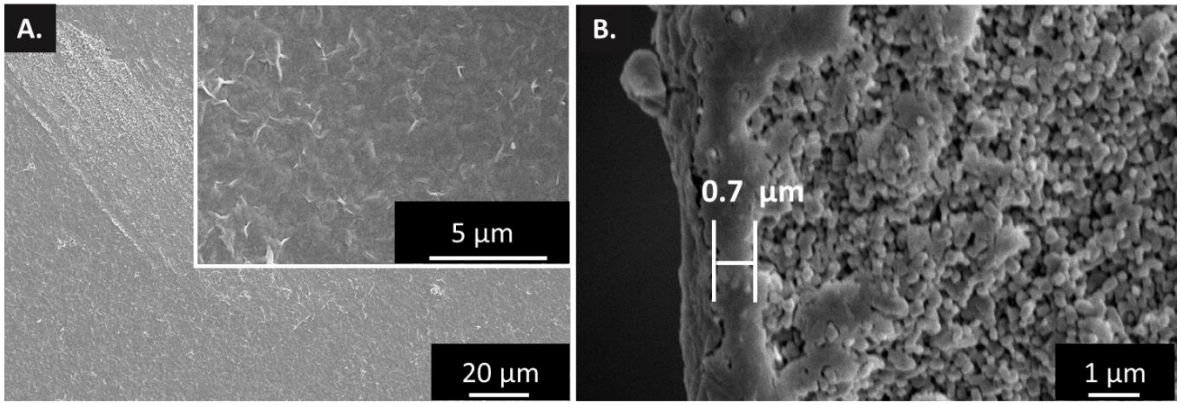

Figure 12. SEM image of 2D $Ni(OH)_2$ nanosheet membrane on α-Al_2O_3 support. (A.) Top surface of membrane. (B.) Cross section of membrane.

Water permeation measurements were conducted to confirm the formation of a 2D nanosheet separation layer on top of the support. Figure 13 shows the water flux of the NiEx and the α-Al_2O_3 support as function of the applied trans-membrane pressure (TMP), ΔP from 4-6 bar. The permeability of the membrane was calculated as the slope of the TMP versus the flux curve. A decrease of 16% for the water permeability was observed for the NiEx compared to the α-Al_2O_3 support (from 5.6 to 4.7 L m^{-2} h^{-1} bar^{-1}). This result suggest the presence of a 2D $Ni(OH)_2$ nanosheet layer.

A retention test of PEG molecules with different molecular weights was carried out to characterize the membrane. These molecules are used commonly to evaluate the molecular-weight cut-off (MWCO) of NF and UF membranes [33]. Figure 14 shows the PEG retention results of two different membranes. NiEx-3 rejected until 7% and NiEx-4 rejected 15% of PEG molecules with Mw above 3500 Da. Therefore, to determine the MWCO of the membranes a different range of Mw should be employed. Qu and co-workers [5] estimated the MWCO on their $Ni(OH)_2$ nanosheet membrane prepared by alkaline co-precipitation filtering solutions of organic dyes with different molecular weights. They reported that the 3.1 µm thick membrane had a MWCO of 328 g mol^{-1} and the lamellar spacing between the nanosheets was 0.86 nm. Nagakawa and co-workers [17] determined the PEG MWCO of niobate (NbO) nanosheet membranes, they reported values of 4.3 and 17 kDa for membranes with thickness of respectively 20 and 70 nm. The PEG MWCO obtained is in the range of ultrafiltration rather than nanofiltration. The same membrane presented promising dyes rejection properties (values). Therefore, the PEG MWCO obtained for the $Ni(OH)_2$ membranes suggested a retention based on charge separation and not molecular sieving.

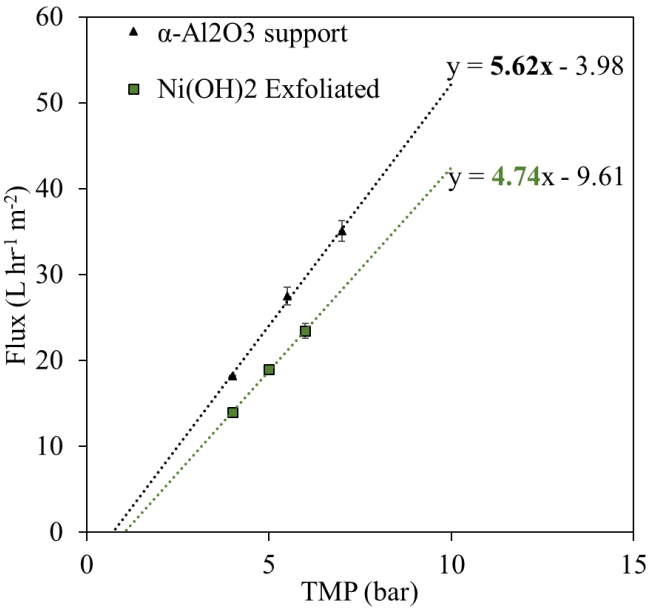

Figure 13. Water permeation of the NiEx membrane and α-Al_2O_3 support at different pressures. The standard deviation was calculated from at least three different samples to obtain the error bars.

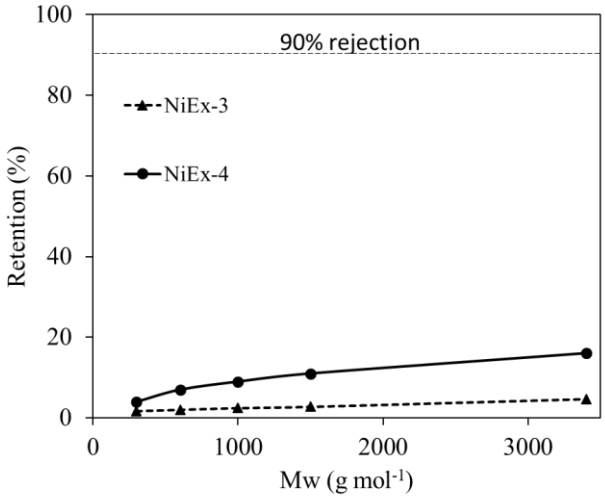

Figure 14. PEG-MWCO measurement of the membranes NiEx-3 and NiEx-4.

To confirm this hypothesis, the rejection performance of NiEx was further studied using Methylene Blue dye (Mw 319.85 g mol^{-1}, aqueous solution at 20 ppm) on a period of 11 hours. This test allowed us to define the separation mechanism of the membrane (e.g. size sieving or adsorption). The different permeate collected as well as the UV/vis spectra are presented in Figure 15 A and D. At the beginning of the test, the first milliliter ($V \leq 2$ mL) of the permeate showed good methylene blue rejection properties (up to 90% of the dye from the feed solution was removed). The methylene blue rejection properties decreased progressively in time, see Figure 15 C. We attribute the methylene blue removal efficiency of the membrane to adsorption rather than size selective effect. The affinity between methylene blue and NiEx could be a result of dipole-dipole interactions

[34]. Once, the membrane is saturated, the methylene blue can pass through the membrane. Qu and co-workers [5] performed methylene blue rejection test on $Ni(OH)_2$ nanosheet membranes prepared on a 200 nm-pore support (Anodisc and Nuclepore track-etch membrane, Whatman), and reported a removal of methylene blue of 95% with a 3.1 µm thick membrane. This removal efficiency is attributed to a selective sieving effect. Also, they performed separation test for direct yellow (DY) dye on membranes with different thicknesses (0.5-3.1 µm), where the removal efficiency goes from 70% for the thinnest membrane to 97% for the thickest always collecting the same permeate volume (20 mL). The removal efficiency is attributed to rejection, without considering the higher surface area of $Ni(OH)_2$ in the thickest membrane, which could enhance adsorption rather than rejection.

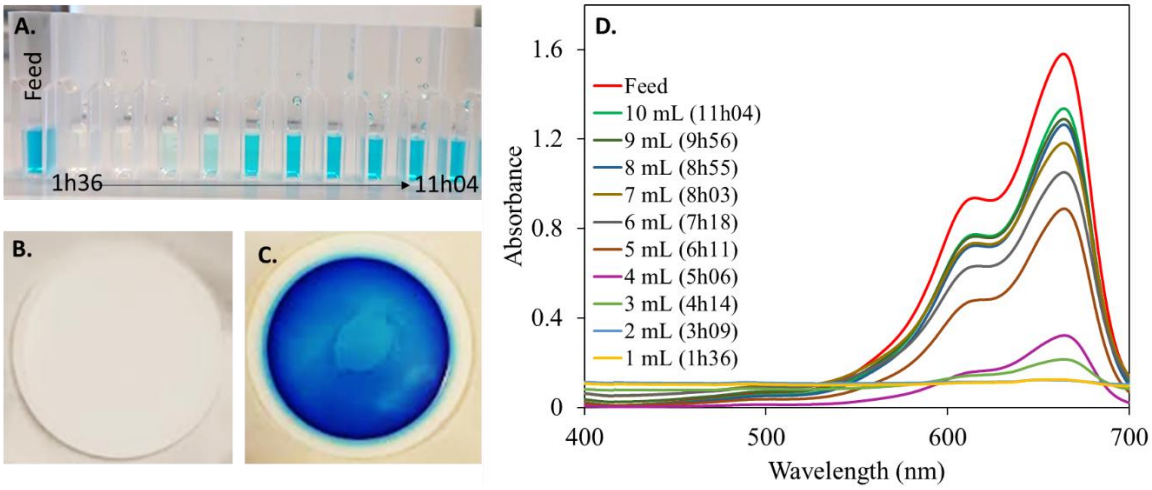

Figure 15. Methylene blue rejection measurement of NiEx. (A.) The feed solution in the left and various permeates. (B.) & (C.) Image of 2D $Ni(OH)_2$ nanosheet membrane before and after filtration of methylene blue solution. (D.) UV/vis spectra of the methylene blue feed solution and various permeates.

The vacuum assisted filtration of 2D $Ni(OH)_2$ nanosheets to for a nanofiltration membrane on α-Al_2O_3 support must be improved to obtain higher homogeneity of the separation layer. A modification in the deposition technique could improve de 2D $Ni(OH)_2$ nanosheets distribution on surface of the support. The use of polymeric support resistant to N-N-dimethylformamide, such like polytetrafluoroethylene, polypropylene, or nylon, could increase the permeability of the nanofiltration membrane. In addition, a functionalization of the surface should be considered to avoid adsorption effect.

A.3. $Ni(OH)_2$ membrane prepared by in situ growth

Most of the 2D inorganic nanosheet based membranes comprise exfoliation to get ultrathin layered structures followed by a deposition on a porous substrate. However,

shortcomings as fragmentation, morphological damage, and reaggregation often occurs by this method. Besides, the exfoliation-deposition method process is unsuitable for large-scale fabrication since these methods are just adapted for flat substrates applicable only for dead-end filtration. The deposition of nanosheets on tubular substrates is more desirable in order to get more stable membranes adapted for cross-flow filtration [10]. To get a first approach of $Ni(OH)_2$ nanosheet membrane adapted for crossflow filtration, we carried out an in situ growth on an α-Al_2O_3 support based on the work from Wang and co-workers [7] for the $Ni(OH)_2$ synthesis and the work from Liu and co-workers[9] for the in situ growth. After synthesis, the α-Al_2O_3 support presented a slight greenish coloration on the top surface, thus confirming the adhesion of $Ni(OH)_2$ to the surface (Figure A. 5). The chemical composition of the growth layer was confirmed by FTIR (see Figure A. 12).

Water permeation measurements were conducted on the resulting membranes and compared with the permeability of the α-Al_2O_3 support. Figure 16 shows that the permeability of the membrane is just 1% lower than the support. Liu and co-workers[9] developed an α-$Co(OH)_2$ nanosheet membrane supported on tubular alumina for organic solvent nanofiltration. They reported a water flux of 120 L $h^{-1}m^{-2}$ for an operation pressure of 5 bar, 81% higher than the flux achieved in this work. This could be a result of the pore size of the support since, the flux of their pristine support is 190 times higher than ours. Moreover, the reduction in flux of the α-$Co(OH)_2$ nanosheet membrane is 84% compared to their pristine support.

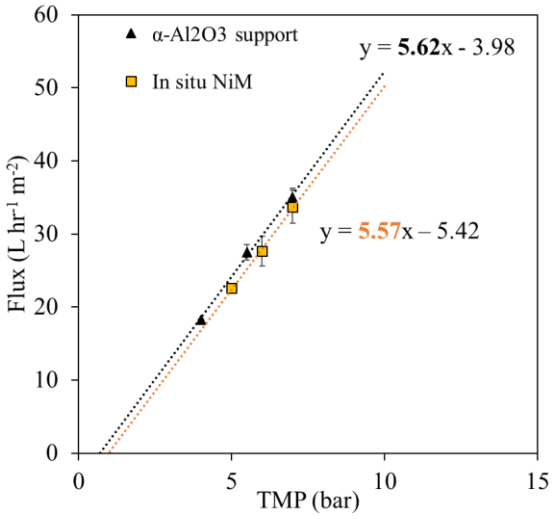

Figure 16. Water permeation of $Ni(OH)_2$ membrane by in situ growth and the pristine α-Al_2O_3 support at different pressures. Standard deviation was estimated from at least three different samples to obtain the error bars.

PEG retention measurements were conducted on the $Ni(OH)_2$ membranes made by in situ growth. Figure 17 shows the results, a maximum retention of 6% was obtained. This low rejection properties can be due to an ineffective coating. In that case, the MWCO would correspond to the one from the α-Al_2O_3 support, which must be in the ultrafiltration range (20 kDa < MWCO > 100 kDa) [35].

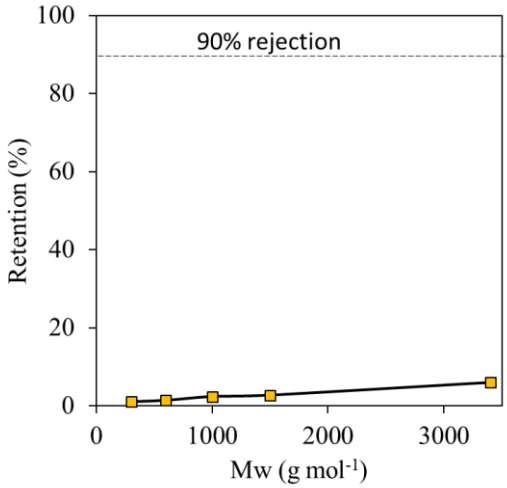

Figure 17. PEG-MWCO of $Ni(OH)_2$ membranes by in situ growth.

To demonstrate the insufficient $Ni(OH)_2$ in-situ growth on/in the α-Al_2O_3 support and to characterize the morphology of the membrane, a SEM analysis was carried out. Figure 18 A shows how a perpendicular multi-layered structure was formed on the surface of the α-Al_2O_3 grain. When the resolution of the image is increased, the incomplete coverage of the α-Al_2O_3 support is confirmed. Liu and co-workers [9] achieved a completely homogeneous α-$Co(OH)_2$ nanosheet membrane by in situ growth by making a pre-coating of the support with polydopamine (PDA) to functionalize the membrane with -OH groups and increase the affinity of the nanosheets for the alumina surface.

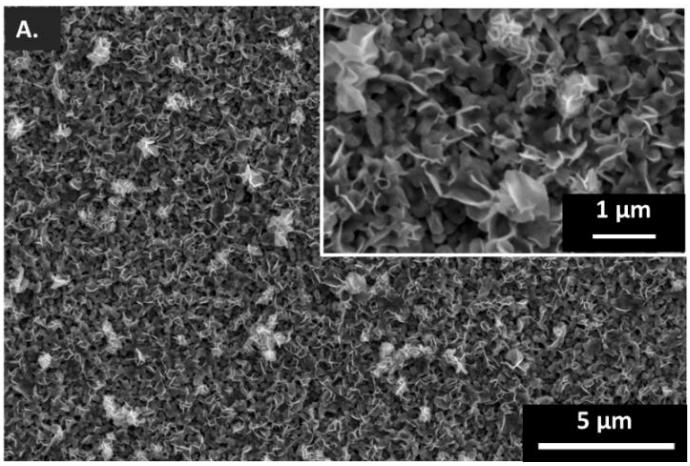

Figure 18. SEM image of surface from the $Ni(OH)_2$ membranes by in situ growth.

In situ growth is a first approach to achieve a stabilized nanosheet based membrane for OSNF with ultrahigh flux. In the case of $Ni(OH)_2$, the technique must be improved either by pre-functionalization of the pristine support surface or by playing with the concentration of Ni(II) salt.

B. 2D-based functionalized BN nanosheet membranes

B.1. 2D functionalized BN nanosheet dispersion

Commercial *h*-BN was exfoliated in presence of urea as the functionalizing agent as described by Chen and co-workers [19]. The functionalization with amino groups enables the dispersion of the h-BN nanosheets in water. The 2D functionalized and exfoliated BN nanosheets were further dissolved in water (400 mL) and the excess of urea was removed by dialysis. Finally, the suspension was centrifuged to remove the non-exfoliated BN.

The successful removal of urea by dialysis was corroborated by FTIR analysis. The FTIR spectrum shown in Figure 19 present two strong bands at 1358 and 775 cm^{-1} assigned respectively to the stretching vibration of the B-N in plane and B-N-B out-of-plane bonds [19,36]. Yang and co-workers [36] demonstrated the successful functionalization of BN nanosheets following an exfoliation and functionalization by planetary ball-milling process under N_2 atmosphere. Their FTIR spectrum presented a peak around 3207 cm^{-1} demonstrating thus the presence of $-NH_2$ groups. In our case, the band is absent, suggesting thus the absence of $-NH_2$ functional groups.

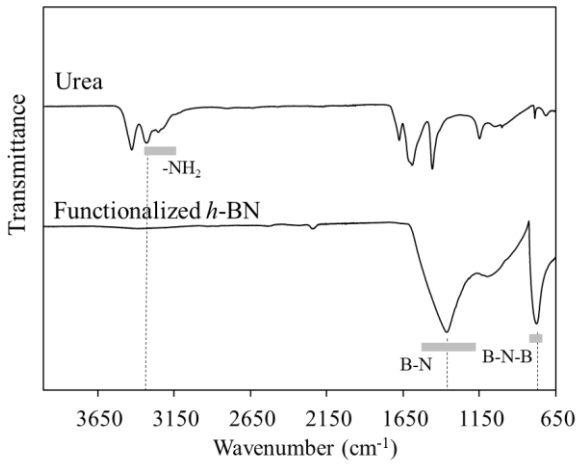

Figure 19. FTIR spectra of clean functionalized 2D BN nanosheets compared with commercial urea.

The STEM-in-SEM mode was used to characterize the morphology and the size of the 2D functionalized BN nanosheets. Figure 20 A shows the STEM-in-SEM image. The nanosheets present an irregular shape and width ≤ 100 nm. The nanosheets are not separated enough to perform a size distribution with ImageJ software. A DLS analysis was performed to get a size distribution and compare with the size detected by STEM-in-SEM. Figure 20 B shows that the nanosheets size distribution obtained by DLS starts at 58 nm and finishes at 300 nm, with particles in maximum concentration at 91 nm. Chen and co-workers [19] measured the functionalized BN nanosheets with AFM, showing a width between 100 and 300 nm.

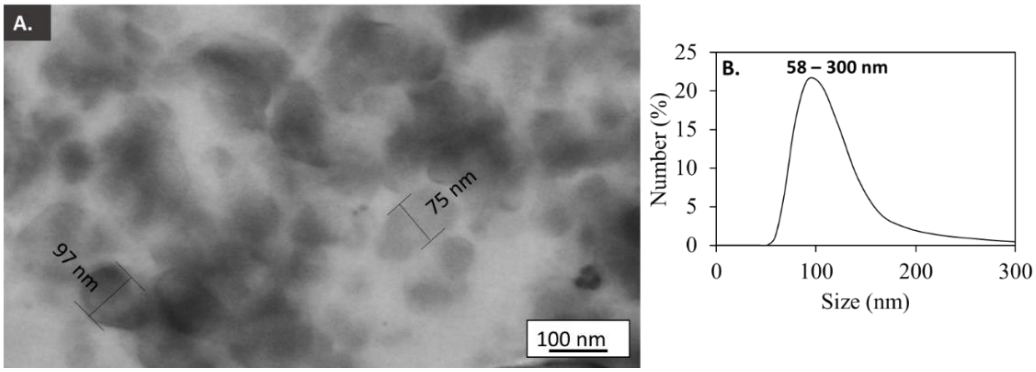

Figure 20. Size and morphology characterization of 2D functionalized BN nanosheets. (A.) STEM-in-SEM image. (B.) Particle size distribution by DLS.

The successful functionalization of the 2D BN nanosheets is unclear from the point of view of the FTIR analysis. However, some traces of amino groups could be present. An XPS analysis could detect the actual concentration of amino groups in the exfoliated nanosheets.

B.2. 2D functionalized BN nanosheet based membranes prepared by vacuum assisted filtration

The 2D functionalized BN nanosheets were deposed on a PES support ($Ø_{pore} \approx 200$ nm) by vacuum assisted filtration. SEM microscopy was used to characterize the membrane morphology and thickness. Figure 21 A shows the top surface of the deposited membrane. The image allows us to appreciate the self-stacked nanosheets forming a homogeneous layer on the PES support. The resulting membrane thickness is approximately 1 µm as shown in Figure 21 B. Chen and co-workers [19] developed membranes with thickness from 0.4 to 8 µm. By changing the volume of dispersion to filtrate, they controlled the final membrane thickness.

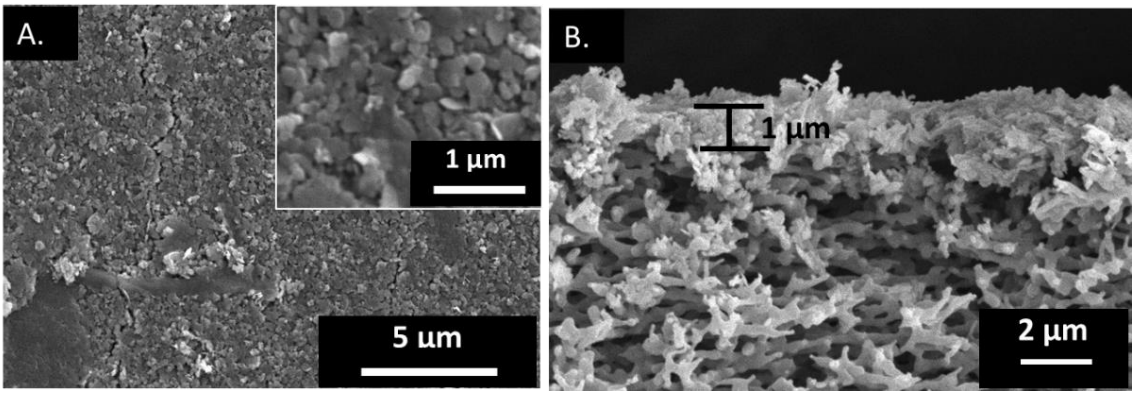

Figure 21. SEM image of the FBNM. (A.) Top surface. (B.) Cross-section.

Water permeation measurements were conducted on the resulting membranes to confirm the formation of a 2D nanosheet separation layer on top of the PES support and measure the water permeability. Figure 22 shows a water flux of 660 L $h^{-1}m^{-2}bar^{-1}$, which is comparable to literature. Chen and co-workers [19] reported a permeance for the 2 µm thick membrane of 620 L $h^{-1}m^{-2}bar^{-1}$, which also presented a better stability after the repetition of multiple test in comparison with thinner membranes.

The rejection performance of FBNMs was studied using methylene blue dye solution at 20 ppm on a period of 5 minutes to define the separation mechanism of the membrane. The different permeate collected as well as the UV/vis spectra are present in Figure 23 A and D. At the beginning of the test, the first millilitres ($V \leq 2$ mL) of the permeate showed good methylene blue rejection properties (up to 95% of the dye from the feed solution was removed). The methylene blue rejection properties decreased progressively until the permeate was as concentrated as the feed ($V \leq 10$ mL). This is because the methylene blue is being adsorbed during the first seconds of filtration, once the nanosheet membrane is saturated, the dye passes through the membrane. Figure 23 C shows the membrane after methylene blue rejection test. The affinity between methylene blue and the BN nanosheets could be due dipole-dipole or π-stacking interactions [34]. Chen an co-workers [19] performed methylene blue rejection test on functionalized BN nanosheet membranes of different thicknesses prepared on a 200 nm-pore support (Nylon microfiber filters). The membranes showed a rejection efficiency of 50%, 60% and 93% for the membranes with thickness of 0.4, 2 and 8 µm respectively. This removal efficiency is attributed to a selective sieving mechanism. Liu and co-workers [34] tested methylene blue removal efficiency on a multifunctional composite membrane based on polyvinylidene fluoride and BN (PVDF/BN). The membrane showed a good removal efficiency at the initial stage of the filtration and a gradual coloration of the permeate

while the process advances. The selectivity of the composite membrane in this case was attributed to physisorption.

PEG retention measurements were conducted on the FBNMs. However, no rejection was observed in the Mw range employed (300 – 3400 Da).

The FBNMs prepared in this work demonstrated lack of real selectivity. This could be a result of the incomplete functionalization of the nanosheets due the lack of a proper milling system. The adsorption of methylene blue on the membrane could be replace by a sieving mechanism with a proper functionalization of the *h*-BN nanosheets.

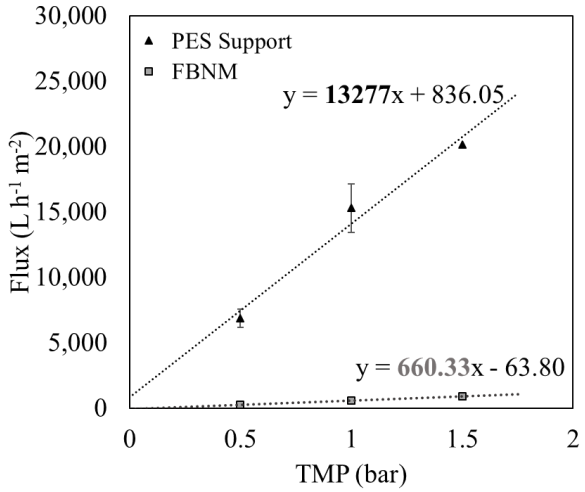

Figure 22. Water permeation of FBNMs and PES support at different pressures. The Standard deviation was estimated from at least three different samples to obtain the error bars.

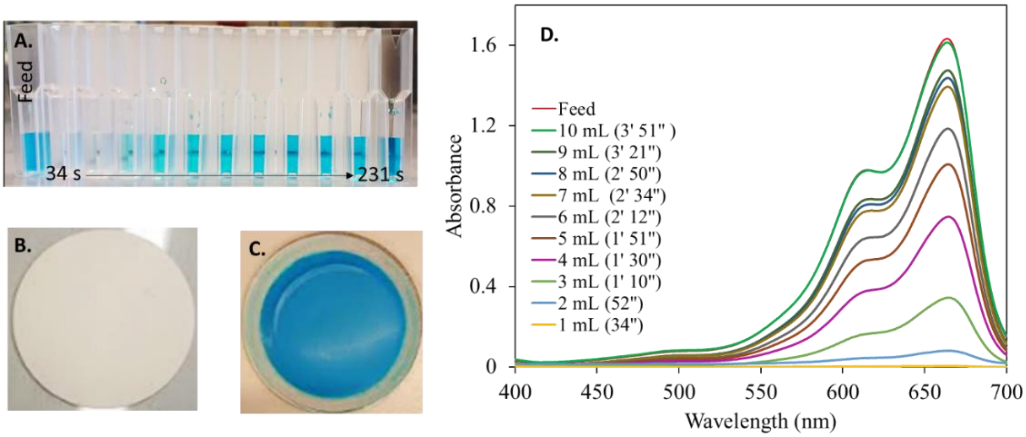

Figure 23. Methylene blue rejection measurement of FBNMs. (A.) The feed solution in the left and various permeates. (B.) & (C.) Image of FBNMs before and after filtration of methylene blue solution. (D.) UV/vis spectra of the methylene blue feed solution and various permeates.

4. Conclusions and Outlook

The synthesis of layered $Ni(OH)_2$ under hydrothermal conditions in presence of a surfactant, as described by Wang et al.[37] enables the formation of a stable 2D crystalline structure, resistant to exfoliation. Thanks to this structural stability, it is possible to get large individual nanosheets (width ≤ 100 nm), which can be further deposited on a porous support to form a membrane. The membranes presented relatively high permeation properties for water (permeability ≈ 4.74 L $hr^{-1}m^{-2}bar^{-1}$) considering the permeation of the α-Al_2O_3 support (permeability ≈ 5.62 L $hr^{-1}m^{-2}bar^{-1}$). However, the rejection properties presented lack of reproducibility and efficiency (R_{NiEx3} ≈ 7% and R_{NiEx3} ≈ 15% for PEG of 3400 Da) may be due the lack of a proper vacuum assisted filtration set-up which allows the formation of a homogeneous separation layer on a ceramic support. Also, a modification on the deposition technique of the suspension could improve the self-stacking of the NiEx on the porous ceramic surface. Once improved the membrane formation of the 2D $Ni(OH)_2$ nanosheet membrane, the selectivity could be improved by playing with size of the interlayer surfactant and functionalization of the surface to avoid dipole-dipole interactions.

The in situ growth of 2D $Ni(OH)_2$ led to the formation of a perpendicular multi-layered structure on the surface of the α-Al_2O_3, as demonstrated with the SEM analysis. The resulting $Ni(OH)_2$ membranes presented several defects affecting their rejection performance (R ≈ 6% for PEG of 3400 Da). In order to increase the affinity of the forming material on the ceramic surface, a pre functionalization of the support could be performed before the in-situ growth synthesis as described by Liu et al. [9].

The preparation of functionalized *h*-BN nanosheets with urea with ball milling was not as effective as expected. The FTIR spectrum suggested that no -NH_2 groups are present on the *h*-BN nanosheets. The forming membranes presented a water permeability as high as that one reported by Chen and co-workers[19] (permeability ≈ 660 L $hr^{-1}m^{-2}bar^{-1}$). The lack of a proper functionalization of the *h*-BN nanosheets could be the reason of the low selectivity of the resulting membrane.

Methylene blue rejection was tested in both $Ni(OH)_2$ and BN based membranes. The results suggest that the removal efficiency of organic dyes in of both membranes is a result of adsorption mechanism rather than selective sieving effect. To be able to measure the retention of dyes, the charges could be neutralized to diminish the adsorption

and enhance the selective sieving mechanism. For example, by the right functionalization of the membrane surface.

5. Bibliography

[1] T. Nakato, J. Kawamata, S. Takagi, Materials Chemistry of Inorganic Nanosheets—Overview and History, in: T. Nakato, J. Kawamata, S. Takagi (Eds.), Inorg. Nanosheets Nanosheet-Based Mater. Fundam. Appl. Two-Dimens. Syst., Springer Japan, Tokyo, 2017: pp. 3–31. doi:10.1007/978-4-431-56496-6_1.

[2] R. Ma, T. Sasaki, Nanosheets of Oxides and Hydroxides: Ultimate 2D Charge-Bearing Functional Crystallites, Adv. Mater. (2010). doi:10.1002/adma.201001722.

[3] J.L. Gunjakar, I.Y. Kim, J.M. Lee, Y.K. Jo, S.-J. Hwang, Exploration of Nanostructured Functional Materials Based on Hybridization of Inorganic 2D Nanosheets, J. Phys. Chem. C. 118 (2014) 3847–3863. doi:10.1021/jp410626y.

[4] Y. Xu, K. Kominami, Y. Ishikawa, Q. Feng, Layered hydroxide nickel benzoates: Hydrothermal synthesis, structure characterization, and exfoliation reaction, J. Colloid Interface Sci. 386 (2012) 107–113. doi:10.1016/j.jcis.2012.07.046.

[5] Y. Qu, Q.G. Zhang, F. Soyekwo, R.S. Gao, R.X. Lv, C.X. Lin, M.M. Chen, A.M. Zhu, Q.L. Liu, Nickel hydroxide nanosheet membranes with fast water and organics transport for molecular separation, Nanoscale. 8 (2016) 18428–18435. doi:10.1039/C6NR06612G.

[6] H. Ang, L. Hong, Engineering defects into nickel-based nanosheets for enhanced water permeability, J. Mater. Chem. A. 5 (2017) 20598–20602. doi:10.1039/C7TA06908A.

[7] D. Wang, W. Yan, G.G. Botte, Exfoliated nickel hydroxide nanosheets for urea electrolysis, Electrochem. Commun. 13 (2011) 1135–1138. doi:10.1016/j.elecom.2011.07.016.

[8] S. Ida, D. Shiga, M. Koinuma, Y. Matsumoto, Synthesis of Hexagonal Nickel Hydroxide Nanosheets by Exfoliation of Layered Nickel Hydroxide Intercalated with Dodecyl Sulfate Ions, J. Am. Chem. Soc. 130 (2008) 14038–14039. doi:10.1021/ja804397n.

[9] H.-X. Liu, C. Zhao, N. Wang, L. Shu, J. Zhou, S. Ji, J.-R. Li, Nanosheet α-Co(OH)2 composite membranes with ultrathin separation layer for removing dyes from solvent with high flux, Sep. Purif. Technol. 207 (2018) 506–513. doi:10.1016/j.seppur.2018.07.001.

[10] Y. Li, L. Lin, M. Tu, P. Nian, A.J. Howarth, O.K. Farha, J. Qiu, X. Zhang, Growth of ZnO self-converted 2D nanosheet zeolitic imidazolate framework membranes by an ammonia-assisted strategy, Nano Res. 11 (2018) 1850–1860. doi:10.1007/s12274-017-1803-0.

[11] X.Q. Cheng, Z.X. Wang, X. Jiang, T. Li, C.H. Lau, Z. Guo, J. Ma, L. Shao, Towards sustainable ultrafast molecular-separation membranes: From conventional polymers to emerging materials, Prog. Mater. Sci. 92 (2018) 258–283. doi:10.1016/j.pmatsci.2017.10.006.

[12] C.N.R. Rao, K. Gopalakrishnan, U. Maitra, Comparative Study of Potential Applications of Graphene, MoS2, and Other Two-Dimensional Materials in Energy Devices, Sensors, and Related Areas, ACS Appl. Mater. Interfaces. 7 (2015) 7809–7832. doi:10.1021/am509096x.

[13] S. Bunani, E. Yörükoğlu, G. Sert, Ü. Yüksel, M. Yüksel, N. Kabay, Application of nanofiltration for reuse of municipal wastewater and quality analysis of product water, Desalination. 315 (2013) 33–36. doi:10.1016/j.desal.2012.11.015.

[14] A.W. Mohammad, Y.H. Teow, W.L. Ang, Y.T. Chung, D.L. Oatley-Radcliffe, N. Hilal, Nanofiltration membranes review: Recent advances and future prospects, Desalination. 356 (2015) 226–254. doi:10.1016/j.desal.2014.10.043.

[15] W.J. Koros, Y.H. Ma, T. Shimidzu, Terminology for membranes and membrane processes (IUPAC Recommendations 1996), Pure Appl. Chem. 68 (2009) 1479–1489. doi:10.1351/pac199668071479.

[16] W. Gao, H. Liang, J. Ma, M. Han, Z. Chen, Z. Han, G. Li, Membrane fouling control in ultrafiltration technology for drinking water production: A review, Desalination. 272 (2011) 1–8. doi:10.1016/j.desal.2011.01.051.

[17] K. Nakagawa, H. Yamashita, D. Saeki, T. Yoshioka, T. Shintani, E. Kamio, H.T. Kreissl, S.C.E. Tsang, S. Sugiyama, H. Matsuyama, Niobate nanosheet membranes with enhanced stability for nanofiltration, Chem. Commun. 53 (2017) 7929–7932. doi:10.1039/C7CC03911E.

[18] G. Liu, W. Jin, N. Xu, Two-Dimensional-Material Membranes: A New Family of High-Performance Separation Membranes, Angew. Chem. Int. Ed. 55 (2016) 13384–13397. doi:10.1002/anie.201600438.
[19] C. Chen, J. Wang, D. Liu, C. Yang, Y. Liu, R.S. Ruoff, W. Lei, Functionalized boron nitride membranes with ultrafast solvent transport performance for molecular separation, Nat. Commun. 9 (2018) 1902. doi:10.1038/s41467-018-04294-6.
[20] Y. Wei, Y. Zhang, X. Gao, Z. Ma, X. Wang, C. Gao, Multilayered graphene oxide membranes for water treatment: A review, Carbon. 139 (2018) 964–981. doi:10.1016/j.carbon.2018.07.040.
[21] C.-H. Tsou, Q.-F. An, S.-C. Lo, M. De Guzman, W.-S. Hung, C.-C. Hu, K.-R. Lee, J.-Y. Lai, Effect of microstructure of graphene oxide fabricated through different self-assembly techniques on 1-butanol dehydration, J. Membr. Sci. 477 (2015) 93–100. doi:10.1016/j.memsci.2014.12.039.
[22] A. Julbe, J.D.F. Ramsay, Chapter 4 Methods for the characterisation of porous structure in membrane materials, in: A.J. Burggraaf, L. Cot (Eds.), Membr. Sci. Technol., Elsevier, 1996: pp. 67–118. doi:10.1016/S0927-5193(96)80007-6.
[23] L. Sun, Y. Ying, H. Huang, Z. Song, Y. Mao, Z. Xu, X. Peng, Ultrafast Molecule Separation through Layered WS2 Nanosheet Membranes, ACS Nano. 8 (2014) 6304–6311. doi:10.1021/nn501786m.
[24] L. Sun, H. Huang, X. Peng, Laminar MoS2 membranes for molecule separation, Chem. Commun. 49 (2013) 10718–10720. doi:10.1039/C3CC46136J.
[25] Y. Liu, N. Wang, J. Caro, In situ formation of LDH membranes of different microstructures with molecular sieve gas selectivity, J. Mater. Chem. A. 2 (2014) 5716–5723. doi:10.1039/C4TA00108G.
[26] S. Yu, X. Wang, H. Pang, R. Zhang, W. Song, D. Fu, T. Hayat, X. Wang, Boron nitride-based materials for the removal of pollutants from aqueous solutions: A review, Chem. Eng. J. 333 (2018) 343–360. doi:10.1016/j.cej.2017.09.163.
[27] W. Lei, V.N. Mochalin, D. Liu, S. Qin, Y. Gogotsi, Y. Chen, Boron nitride colloidal solutions, ultralight aerogels and freestanding membranes through one-step exfoliation and functionalization, Nat. Commun. 6 (2015) 8849. doi:10.1038/ncomms9849.
[28] D. Liu, M. Zhang, L. He, Y. Chen, W. Lei, Layer-by-Layer Assembly Fabrication of Porous Boron Nitride Coated Multifunctional Materials for Water Cleaning, Adv. Mater. Interfaces. 4 (2017) 1700392. doi:10.1002/admi.201700392.
[29] S. Qin, D. Liu, Y. Chen, C. Chen, G. Wang, J. Wang, J.M. Razal, W. Lei, Nanofluidic electric generators constructed from boron nitride nanosheet membranes, Nano Energy. 47 (2018) 368–373. doi:10.1016/j.nanoen.2018.03.030.
[30] J.W. Mullin, Crystallization, Elsevier, 2001.
[31] T. Nakato, Synthetic Nanosheets from Ion-Exchangeable Layered Solids, in: T. Nakato, J. Kawamata, S. Takagi (Eds.), Inorg. Nanosheets Nanosheet-Based Mater. Fundam. Appl. Two-Dimens. Syst., Springer Japan, Tokyo, 2017: pp. 55–100. doi:10.1007/978-4-431-56496-6_3.
[32] J.M. Dreyfors, S.B. Jones, Y. Sayed, Hexamethylenetetramine: A Review, Am. Ind. Hyg. Assoc. J. 50 (1989) 579–585. doi:10.1080/15298668991375191.
[33] M.-A. Pizzoccaro-Zilamy, C. Huiskes, E.G. Keim, S.N. Sluijter, H. van Veen, A. Nijmeijer, L. Winnubst, M.W.J. Luiten-Olieman, New Generation of Mesoporous Silica Membranes Prepared by a Stöber-Solution Pore-Growth Approach, ACS Appl. Mater. Interfaces. 11 (2019) 18528–18539. doi:10.1021/acsami.9b03526.
[34] D. Liu, L. He, W. Lei, K.D. Klika, L. Kong, Y. Chen, Multifunctional Polymer/Porous Boron Nitride Nanosheet Membranes for Superior Trapping Emulsified Oils and Organic Molecules, Adv. Mater. Interfaces. 2 (2015) 1500228. doi:10.1002/admi.201500228.
[35] Ultrafiltration, Nanofiltration and Reverse Osmosis, Safe Drink. Water Found. (n.d.). https://www.safewater.org/fact-sheets-1/2017/1/23/ultrafiltrationnanoandro (accessed June 21, 2019).

[36] C. Yang, D. Liu, Y. Chen, C. Chen, J. Wang, Y. Fan, S. Huang, W. Lei, Three-Dimensional Functionalized Boron Nitride Nanosheets/ZnO Superstructures for CO2 Capture, ACS Appl. Mater. Interfaces. 11 (2019) 10276–10282. doi:10.1021/acsami.8b20775.
[37] L. Wang, C. Lin, D. Huang, J. Chen, L. Jiang, M. Wang, L. Chi, L. Shi, J. Jin, Optimizing the Volmer Step by Single-Layer Nickel Hydroxide Nanosheets in Hydrogen Evolution Reaction of Platinum, Acs Catal. 5 (2015) 3801–3806. doi:10.1021/cs501835c.